Vol. 25, No. 3(2026) Sim26886

Revista Mexicana de Ingeniería Química

Variable-order fractional diffusion-reaction in porous catalyst pellets under progressive deactivation: A numerical comparative study

Difusión-reacción fraccional de orden variable en pellets catalíticos porosos bajo desactivación progresiva: un estudio numérico comparativo

R. Soto-Soto[1], L. Vicente[2], and A.E. Rodriguez-Mata[3*]

[1]Universidad Tecnológica de México – UNITEC México, Campus Ecatepec, Ecatepec de Morelos, Estado de México, México.

[2]Departamento de Física y Química Teórica, Facultad de Química, Universidad Nacional Autónoma de México, 04510 México, CDMX, México.

[3]Tecnológico Nacional de México / Instituto Tecnológico de Chihuahua, Av. Tecnológico 2909, Col. 10 de Mayo, C.P. 31200, Chihuahua, Chihuahua, México.

Sent: May 31, 2026; Accepted: September 1, 2026

Abstract

Classical diffusion-reaction models for porous catalyst pellets usually assume Fickian transport with constant effective diffusivity. However, catalyst deactivation caused by coke deposition, fouling, poisoning, or sintering progressively modifies the pore network and may induce anomalous subdiffusive transport. In this work, a variable-order fractional diffusion-reaction model is proposed for an isothermal flat-slab catalyst pellet with a first-order irreversible reaction. The classical time derivative is replaced by a Caputo derivative of time-dependent order $\alpha(\tau)$, described by phenomenological exponential law $\alpha(\tau) = \alpha_\infty + (1-\alpha_\infty)\exp(-\lambda\tau)$, which represents the transition from fresh Fickian transport to aged subdiffusive behavior. The model is solved using an implicit L1 finite-difference scheme and compared with the classical Crank–Nicolson solution. The transient catalyst effectiveness factor is used as the main performance indicator. Numerical results show that the variable-order model predicts slower reactant penetration and lower transient effectiveness during catalyst aging, demonstrating that classical models may overestimate catalyst performance under progressive transport degradation.

Keywords: variable-order fractional calculus; anomalous subdiffusion; catalyst deactivation; effectiveness factor; diffusion-reaction model.

Resumen

Los modelos clásicos de difusión-reacción en pellets catalíticos porosos suelen asumir transporte Fickiano con difusividad efectiva constante. Sin embargo, la desactivación catalítica causada por depósito de coque, ensuciamiento, envenenamiento o sinterización modifica progresivamente la red porosa y puede inducir transporte subdifusivo anómalo. En este trabajo se propone un modelo fraccional de orden variable para un pellet catalítico plano e isotérmico con reacción irreversible de primer orden. La derivada temporal clásica se reemplaza por una derivada de Caputo de orden dependiente del tiempo $\alpha(\tau)$, definida mediante la ley exponencial $\alpha(\tau) = \alpha_\infty + (1-\alpha_\infty)\exp(-\lambda\tau)$, la cual representa la transición desde transporte Fickiano en un catalizador fresco hasta comportamiento subdifusivo en un catalizador envejecido. El modelo se resuelve mediante un esquema implícito L1 de diferencias finitas y se compara con la solución clásica de Crank–Nicolson. El factor de efectividad transitorio se utiliza como indicador principal de desempeño. Los resultados numéricos muestran que el modelo de orden variable predice una penetración más lenta del reactivo y una menor efectividad transitoria durante el envejecimiento catalítico.

Palabras clave: cálculo fraccional de orden variable; subdifusión anómala; desactivación catalítica; factor de efectividad; modelo difusión-reacción.

*Corresponding author. *E-mail*: abraham.rm@chihuahua.tecnm.mx;
https://doi.org/10.24275/rmiq/Sim26886
ISSN:1665-2738, *issn-e*: 2395-8472

1 Introduction

The diffusion-reaction problem in porous catalyst pellets is a fundamental aspect of heterogeneous catalysis and chemical reactor engineering. The classical treatment, originating from the foundational works of Thiele (1939) and Zeldovich (1939), posits that intraparticle transport adheres to Fick's second law, characterised by a constant and isotropic effective diffusivity D_{eff} (Valdés-Parada *et al.*, 2023).

Under this assumption, the problem simplifies to a linear parabolic partial differential equation (PDE) characterised by the Thiele modulus $\phi = L\sqrt{k/D_{\text{eff}}}$. The steady-state solution has a closed analytical form, while the transient solution describes the progression towards steady state (Aris, 1975; Fogler, 2016). The classical effectiveness factor $\eta_\infty = \tanh\phi/\phi$ (for a flat-slab pellet with first-order kinetics) has established itself as a standard design parameter in the engineering of fixed-bed and fluidized-bed reactors (Froment *et al.*, 2011; Levenspiel, 1998). Recent advancements in analytical methods have broadened the scope of reaction-diffusion solutions to encompass finite cylindrical pellets and catalytic particles exhibiting various morphologies within batch reactors and continuous stirred-tank reactors (CSTRs). This underscores the sustained significance of pellet-scale transport models in the context of reactor analysis and design (Y. Cho, 2022; Y.-S. Cho, 2023).

In practice, catalysts experience a gradual decline in activity throughout their operation (Bartholomew, 2001; Moulijn *et al.*, 2001). Coke deposition, fouling, and poisoning due to feed impurities, along with the sintering of metal crystallites, lead to irreversible modifications in the pore network. These changes result in a diminished active surface area, an increase in tortuosity, and the narrowing or obstruction of diffusion pathways (Froment *et al.*, 2011). Recent pore-network modelling has demonstrated that microstructural features, including macroporosity, pore-size ratio, and hierarchical pore connectivity, significantly influence both catalyst performance and deactivation patterns. This highlights that the internal transport resistance evolves in accordance with the catalyst structure, rather than remaining constant during operation (Moghaddama *et al.*, 2022). The overall impact on mass transport is thus insufficiently captured by a singular constant diffusivity. As the pore structure deteriorates, the diffusive flux diverges from the linear Fickian expectation, and D_{eff} increasingly falls short as a descriptor of the transport phenomenon (Keil, 2012). More generally, effective-diffusivity and coupled heat- and mass-transfer models have been successfully employed to describe transport within structured particles and heterogeneous media, highlighting the importance of internal transport properties in determining macroscopic system behavior (Cortés-Avendaño *et al.*, 2023; Martínez-Hilario *et al.*, 2023).

A growing body of experimental and modelling evidence associates these structural changes with anomalous, non-Fickian transport. Recent studies involving catalytic processes in porous media further illustrate the strong coupling between pore-scale transport and reaction phenomena under evolving operating conditions (Birbal *et al.*, 2025). In the study conducted by A. Zhokh and Strizhak (2018), the diffusion of methanol through pelletized zeolite-alumina catalysts was measured, revealing that the standard diffusion equation does not apply. Instead, a time-fractional diffusion equation with an order of $\alpha \approx 0.85$ was found to accurately reproduce the experimental mass-transfer kinetics.According to the findings of A. Zhokh and Strizhak (2019), a consistent spatiotemporal scaling behaviour was observed in mesoporous pellets of different sizes. Structurally, subdiffusion emerges when molecular transport is dictated by power-law waiting-time distributions instead of exponential Poisson waiting times. This phenomenon is physically linked to the trapping of diffusing molecules in dead-end pores, narrow constrictions, or adsorption sites resulting from fouling (Bouchaud and Georges, 1990; Metzler and Klafter, 2000). In this anomalous regime, the mean squared displacement is characterised by the relationship $\langle x^2(t)\rangle \propto t^\alpha$ where $0 < \alpha < 1$. The governing equation is appropriately formulated using a fractional time-derivative of order α (Kilbas *et al.*, 2006; Podlubny, 1999). Recent studies on anomalous diffusion in porous media have reinforced this interpretation by demonstrating that variable-order time-fractional models can effectively capture transport regimes where the memory depth varies with respect to space, time, or material state (Hong *et al.*, 2024; Sobhani *et al.*, 2023; Zhang and Liu, 2023).

Fractional calculus has found applications in diffusion-reaction and mass-transfer problems since the early 2000s, providing alternative frameworks for representing transport processes

that depart from conventional integer-order descriptions (Melgarejo-Torres *et al.*, 2022). In porous catalytic systems, pioneering macrokinetic frameworks incorporating the effects of anomalous diffusion were subsequently proposed. More recently, the group of Hernández-Martínez *et al.*, (2016) developed a formulation based on Green's functions to address fractional reaction-diffusion (FRD) models that incorporate general boundary conditions and nonlinear reaction terms (Hernández-Martínez *et al.*, 2016). They subsequently expanded this framework to assess the isothermal and non-isothermal effectiveness factor of porous catalytic slabs, taking into account non-Fickian diffusion and external mass-transfer resistance (Hernández Aguirre *et al.*, 2017). In the study conducted by Martínez-Martínez *et al.*, (2016), the dynamic effectiveness factor of catalytic particles exhibiting anomalous diffusion was examined through a Cattaneo-type fractional equation. The research employed frequency-domain analysis and Bode diagrams to delineate the conditions that favour dynamic operation over steady-state operation in non-Fickian systems. Recent studies on fractional reaction-diffusion in immobilised enzyme and porous biocatalytic systems have demonstrated that fractional-order formulations can more flexibly represent complex nonlinear kinetics compared to integer-order models, particularly in scenarios where diffusion, reaction, and internal microstructure exhibit strong interactions (Rajaraman, 2024).

The effectiveness factor of the catalyst has been re-examined through the lens of fractional transport. In their study, A. Zhokh and Strizhak (2018) investigated the steady-state reaction-diffusion problem incorporating a space-fractional derivative through the Haar wavelet collocation method. Their findings reveal a significant dependence of the effectiveness factor and the necessary reactor volume on the anomalous diffusion exponent. This line of research has recently been expanded to include the direct modelling of catalyst effectiveness factors using space-fractional derivatives, offering further evidence that anomalous diffusion can substantially alter the apparent performance of porous catalysts (O. Zhokh, 2024). Nevertheless, the majority of existing fractional models for catalytic pellets exhibit a fundamental constraint: the fractional order α is typically assumed to remain constant over the duration of the catalyst's lifetime. This presents physical limitations for the deactivation of catalysts. In a newly synthesised catalyst, the pore structure exhibits a relatively uniform arrangement, and the transport mechanism is predominantly Fickian ($\alpha \approx 1$). As deactivation advances, the gradual blockage of pores, constriction, and loss of connectivity lead to the extensive waiting-time distributions that characterise subdiffusion; it is only at a later stage of deactivation that α nears an asymptotic value $\alpha_\infty < 1$. Modelling this process with a fixed α selected *ad hoc* is consequently analogous to presuming that the catalyst is perpetually fresh or entirely deactivated, both of which fail to accurately depict the transient operation of an actual catalytic reactor.

Coking and fouling are not purely local-in-time phenomena: precursor deposition and pore blockage are also known to develop unevenly across the pellet radius, so that the near-surface region typically ages faster than the pellet core (Bartholomew, 2001; Froment *et al.*, 2011). A fully general description would therefore require a fractional order $\alpha(\xi,\tau)$ depending on both position and time, coupling spatial heterogeneity of trapping sites with temporal memory. In this first study we deliberately restrict the scope to a spatially uniform, time-dependent order $\alpha(\tau)$ for two reasons. First, the experimental evidence motivating this work (A. Zhokh and Strizhak, 2018; A. Zhokh and Strizhak, 2019) reports a single time-fractional order fitted from pellet-averaged mass-uptake curves, without spatially resolved information that could constrain a two-variable $\alpha(\xi,\tau)$; introducing spatial dependence beyond what the data support would add unconstrained degrees of freedom. Second, isolating the temporal evolution of α allows the aging mechanism to be decoupled from the spatial transport operator, so that its effect on the transient effectiveness factor can be identified unambiguously and compared directly against the classical model, which is the primary goal of the present work. Extending the formulation to a space-time variable order $\alpha(\xi,\tau)$ that would also capture the spatial heterogeneity introduced by coke deposition is a natural and important next step, and is discussed explicitly in the outlook of this paper.

Variable-order fractional calculus offers a natural extension necessary for capturing time-evolving anomalies. Introduced by Samko and Ross (1993) and formalised by Lorenzo and Hartley (2002), VO-FDEs substitute the constant exponent α with a function $\alpha(t)$, $\alpha(x)$, or $\alpha(t,x)$, which encapsulates the instantaneous memory depth of the system. According to the work of Sun *et al.*, (2019), a thorough examination of VO-FDE definitions, numerical techniques,

physical models, and their applications is presented. The authors highlight transport in heterogeneous and evolving media as a particularly promising domain for VO-FDE modelling. Applications have been documented in the context of anomalous diffusion within inhomogeneous media (Chechkin *et al.*, 2005), viscoelastic mechanics (Coimbra, 2003), adaptive control strategies (Dabiri *et al.*, 2018), and subsurface flow phenomena (Obembe *et al.*, 2017). Recent advancements have broadened this area to encompass nonlinear diffusion in amorphous materials, variable-order dual-phase-lag transport in porous media, inverse identification of spatially dependent variable order, and distributed-order diffusion with variable coefficients (Hong *et al.*, 2024; Sobhani *et al.*, 2023; Wen *et al.*, 2024; Zhang and Liu, 2023). These investigations substantiate the notion that variable or distributed fractional orders extend beyond mere mathematical abstractions; they serve as practical representations of transport phenomena characterised by memory, heterogeneity, or diffusion mechanisms that evolve with the state of the material.

To the best of our knowledge, variable-order fractional differential equations have not yet been systematically applied to the diffusion-reaction problem in progressively deactivating porous catalyst pellets. Furthermore, there is no published framework that explicitly couples the evolution of the fractional order to the degradation state of the catalyst and the transient effectiveness factor. This gap is noteworthy due to the fact that catalyst deactivation is fundamentally dependent on time, whereas the anomalous transport exponent is anticipated to vary as the pore network develops.

This study tackles the identified gap by introducing, solving, and numerically assessing a variable-order fractional diffusion-reaction model for isothermal transport within a flat-slab catalyst pellet experiencing progressive deactivation. The particular contributions of this work are fourfold. First, we introduce a physically motivated VO-FDE model for catalysis, in which the parameter $\alpha(\tau)$ is determined by an exponential deactivation law, expressed as $\alpha(\tau) = \alpha_\infty + (1-\alpha_\infty)\exp(-\lambda\tau)$; this functional form meets the necessary physical constraint $\alpha(0) = 1$ for fresh, Fickian transport and facilitates a systematic adjustment of the deactivation rate λ and the asymptotic anomaly α_∞. Second, we implement a highly effective implicit numerical method, executing the L1 discretization of the Caputo VO derivative (Sun *et al.*, 2019, Eq. 4.1) within a completely implicit finite-difference framework, which results in a tridiagonal system at each time step that is resolved in $\mathcal{O}(N_x)$ operations. Third, we perform a quantitative analysis in relation to the classical model: the VO-FDE model is addressed concurrently with the classical Crank–Nicolson scheme, and a comparison is made between the two via the transient effectiveness factor $\eta(\tau)$, assessing the relative error between models as a function of time and delineating the conditions under which the classical approximation holds true. Fourth, we carry out a parametric investigation of the deactivation parameters α_∞, λ, and the Thiele modulus ϕ^2, which reveals the critical ranges of each parameter and provides practical criteria for selecting the appropriate model in reactor design.

The paper is structured as follows. The subsection "Mathematical formulation" delineates the governing equations for both the classical integer-order diffusion-reaction model and the proposed variable-order fractional model. The section titled "Numerical methods" delineates the spatial and temporal discretization techniques employed for both formulations, encompassing the Crank–Nicolson and implicit L1 methods. The paragraph "Results and Discussion" provides a numerical comparison of both models, encompassing concentration profiles, transient efficacy factors, parametric analysis, and the influence of the memory kernel.

2 Mathematical formulation

2.1 *Problem statement and dimensionless variables*

Consider a flat-slab (plane geometry) catalyst pellet of half-thickness L with an irreversible first-order reaction A $\rightarrow$ products characterized by the intrinsic rate constant k (units: s^{-1}). The reactant diffuses from the external surface of the pellet (at position $x = L$) toward the symmetry plane (at $x = 0$). We introduce the dimensionless variables:

$$u = \frac{C}{C_s}, \quad \xi = \frac{x}{L}, \quad \tau = \frac{D_{\text{eff}}\, t}{L^2}, \tag{1}$$

where C_s is the reactant concentration at the pellet surface and D_{eff} is the effective diffusivity of the fresh catalyst. The Thiele modulus is defined as

$$\phi^2 = \frac{k\, L^2}{D_{\text{eff}}}, \tag{2}$$

which represents the ratio of the characteristic diffusion time L^2/D_{eff} to the characteristic reaction time k^{-1}. The system is subject to the following initial and boundary conditions:

$$u(\xi,0) = 0, \tag{3}$$

$$\left.\frac{\partial u}{\partial \xi}\right|_{\xi=0} = 0, \tag{4}$$

$$u(1,\tau) = 1. \tag{5}$$

Condition (4) enforces symmetry at the pellet center; (5) sets the surface concentration equal to the constant bulk value (no external mass-transfer resistance).

2.2 Model M_{cl}: Classical integer-order diffusion-reaction

Under the assumption of Fickian transport with constant effective diffusivity, the dimensionless reactant balance in the pellet reads

$$\frac{\partial u}{\partial \tau} = \frac{\partial^2 u}{\partial \xi^2} - \phi^2 u, \quad \xi \in (0,1),\ \tau > 0. \tag{M_{cl}}$$

The steady-state solution of (M_{cl}) is $u_\infty(\xi) = \cosh(\phi\,\xi)/\cosh(\phi)$, yielding the classical Thiele effectiveness factor

$$\eta_\infty = \frac{\tanh\phi}{\phi}. \tag{6}$$

This model constitutes the reference benchmark throughout the paper.

2.3 Model M_{vo}: Variable-order fractional diffusion-reaction

In the VO-FDE model, the integer-order time derivative in (M_{cl}) is replaced by the left Caputo variable-order fractional derivative of order $\alpha(\tau) \in (0,1)$, defined as (Sun *et al.*, 2019, Definition 2.14):

$${}^{C}D^{\alpha(\tau)}_{0,\tau}u(\xi,\tau) = \frac{1}{\Gamma\big(1-\alpha(\tau)\big)}\int_0^\tau \frac{\partial u(\xi,s)}{\partial s}\frac{ds}{(\tau-s)^{\alpha(\tau)}}. \tag{7}$$

Why the Caputo formulation. Among the available fractional operators, the Caputo derivative was selected over the Riemann–Liouville (RL) and Grünwald–Letnikov (GL) definitions for three physically and numerically motivated reasons. First, the Caputo derivative of a constant is zero and requires only the ordinary (integer-order) initial condition $u(\xi,0) = 0$ in (3), whereas the RL derivative requires initial data on a fractional-order quantity (e.g., a fractional integral of u) that has no direct physical meaning for a reactant concentration and cannot be measured or specified from the physical problem. Second, for a function that is well behaved (bounded and differentiable) at $\tau = 0$, as is the case for $u(\xi,\tau)$ starting from the compatible initial state $u(\xi,0) = 0$, the Caputo derivative of a constant vanishes, which prevents the spurious singular behaviour at $\tau \to 0$ that is otherwise produced by the RL operator. Third, the GL definition, although numerically convenient and asymptotically equivalent to the Caputo derivative for sufficiently smooth functions, is most naturally posed on infinite or semi-infinite uniform grids and is less directly compatible with the variable-order extension and with standard finite-difference boundary treatments used here (Kilbas *et al.*, 2006; Podlubny, 1999; Sun *et al.*, 2019). These three considerations, and not merely mathematical convenience, motivate the use of the Caputo formulation (7) throughout this work.

The VO-FDE governing equation is

$${}^{C}D^{\alpha(\tau)}_{0,\tau}u(\xi,\tau) = \frac{\partial^2 u}{\partial \xi^2} - \phi^2 u, \quad \xi \in (0,1),\ \tau > 0, \tag{M_{vo}}$$

subject to the same initial and boundary conditions (3)–(5).

Limiting cases. Two important limits of (M_{vo}) follow directly from the definition of the operator. If $\alpha(\tau) = 1$ for all τ, the operator (7) reduces to the ordinary first-order derivative, and (M_{vo}) recovers the classical model (M_{cl}). If instead $\alpha(\tau) = \alpha_0 = \text{const.} < 1$, ($M_{vo}$) reduces to a constant-order fractional diffusion-reaction equation, as studied in Hernández Aguirre *et al.*, (2017). Thus, (M_{vo}) is a strict generalization of both the classical and the constant-order fractional models.

2.4 Deactivation law for $\alpha(\tau)$ and the dimensionless deactivation constant

A key modeling choice is the functional form of $\alpha(\tau)$. In the present study, we adopt the following phenomenological exponential evolution law, motivated by analogy with first-order catalyst deactivation:

$$\boxed{\alpha(\tau) = \alpha_\infty + (1-\alpha_\infty)e^{-\lambda\tau},} \tag{8}$$

where $\alpha_\infty \in (0,1)$ is the asymptotic fractional order at full deactivation and $\lambda > 0$ is the dimensionless deactivation rate constant.

It is important to emphasize that Eq. (8) is introduced here as a phenomenological modeling

Table 1. Physical interpretation of the parameters in the deactivation law, Eq. (8).

Parameter	Limit	Value of α	Physical meaning
τ	$\tau \to 0$	$\alpha(0) = 1$	Fresh catalyst; Fickian transport
	$\tau \to \infty$	$\alpha(\infty) = \alpha_\infty$	Fully deactivated; anomalous subdiffusion
α_∞	$\alpha_\infty \to 1$	$\alpha(\tau) \approx 1$	Mild deactivation; near-Fickian
	$\alpha_\infty \to 0$	$\alpha(\tau) \to 0$	Severe deactivation; strongly subdiffusive
λ	Large λ	Fast transition to α_∞	Rapid pore blockage (severe coking)
	Small λ	Slow transition to α_∞	Gradual fouling or mild poisoning

hypothesis rather than as an experimentally established constitutive relationship between pore degradation and the fractional order. In the present framework, $\alpha(\tau)$ is used as an effective descriptor of the progressive transition from nearly Fickian to increasingly subdiffusive transport. The exponential form is selected because it satisfies the physically required limits $\alpha(0) = 1$ and $\alpha(\tau \to \infty) = \alpha_\infty$, while introducing only one additional timescale parameter, λ. Its motivation arises from the analogy with first-order catalyst-deactivation kinetics, but the assumption that the anomalous transport order follows the same functional dependence has not yet been experimentally validated. Establishing a constitutive relationship between pore-structure evolution and $\alpha(\tau)$ therefore requires independent experimental validation and is identified as an important direction for future work.

Because τ is itself dimensionless (Eq. (1)), the argument of the exponential in (8) must be dimensionless as well, which fixes λ to be a dimensionless group rather than a dimensional rate. If deactivation in dimensional time t is described by a first-order activity-decay constant k_d (units s^{-1}), i.e. $a(t) = \exp(-k_d t)$ as in classical deactivation kinetics (Bartholomew, 2001; Froment *et al.*, 2011), then writing $t = \tau L^2/D_{\text{eff}}$ shows that the dimensionless deactivation constant used in (8) is

$$\lambda = k_d \frac{L^2}{D_{\text{eff}}}, \tag{9}$$

i.e. the ratio of the characteristic diffusion time L^2/D_{eff} to the characteristic deactivation time k_d^{-1}, in direct analogy with the definition of the Thiele modulus in Eq. (2). A value $\lambda \gg 1$ therefore means that deactivation is fast relative to diffusion (the pellet reaches α_∞ before an appreciable concentration profile develops), while $\lambda \ll 1$ means that diffusion equilibrates the pellet long before appreciable aging occurs.

Regarding the units of the governing equation itself: the classical time derivative $\partial u/\partial \tau$ in (M_{cl}) has units of (dimensionless concentration)/(dimensionless time). Because the Caputo VO derivative of order $\alpha(\tau)$ is defined through a fractional integral of the ordinary derivative (Eq. (7)), the operator ${}^{C}D_{0,\tau}^{\alpha(\tau)} u$ formally carries units of (dimensionless concentration)/(dimensionless time)$^{\alpha(\tau)}$, which vary continuously with τ as $\alpha(\tau)$ evolves. This is compensated in the numerical scheme by the scaling factor $\gamma_k = \Delta\tau^{\alpha_{k+1}}\Gamma(2 - \alpha_{k+1})$ introduced in Eq. (17), which restores a dimensionally consistent algebraic balance at every time step regardless of the instantaneous value of $\alpha(\tau)$; this is analogous to the role played by the generalized diffusivity in constant-order fractional diffusion equations (Podlubny, 1999).

Table 1 summarizes the physical interpretation of the limiting values of the parameters.

The choice of an exponential form for (8) is motivated by analogy with established first-order catalyst-deactivation kinetics, in which the catalyst activity is commonly represented as $a(t) = \exp(-k_d t)$ (Bartholomew, 2001; Froment *et al.*, 2011). Within the present phenomenological framework, the fractional order $\alpha(\tau)$ should therefore be interpreted as an effective descriptor of the evolving transport regime rather than as a direct measure of pore volume, coke concentration, or any other specific microstructural variable. The exponential form provides a simple two-parameter interpolation between the fresh-catalyst limit $\alpha(0) = 1$ and the asymptotic aged-state value α_∞, while allowing the rate of this transition to be controlled by λ. Accordingly, the correspondence between catalyst deactivation and the evolution of $\alpha(\tau)$ is a modeling hypothesis of the present work and should not be interpreted as an experimentally established constitutive relationship.

2.5 *Catalyst effectiveness factor*

The transient catalyst effectiveness factor is defined as the spatial average of the

dimensionless concentration:

$$\eta(\tau) = \int_0^1 u(\xi,\tau)\, d\xi. \tag{10}$$

For a first-order reaction, $\eta(\tau)$ equals the ratio of the actual reaction rate integrated over the pellet volume to the rate that would prevail if the entire pellet were exposed to the surface concentration C_s, i.e., $\eta = \langle r\rangle / r(C_s) = \langle u\rangle$ (Aris, 1975). The steady-state limit η_∞ is given by (6) for model (M_{cl}). For model (M_{vo}), the steady-state is also $\eta_\infty = \tanh\phi/\phi$ (since both models share the same steady-state equation), but the transient approach differs substantially, as shown in the following section.

3 Numerical methods

This section provides a numerical assessment of the suggested variable-order fractional diffusion-reaction model and compares it with the classical integer-order formulation. The research concentrates on measuring the impact of the progressive shift from Fickian transport to anomalous subdiffusion on the transient concentration field within the porous catalyst pellet and, subsequently, on the anticipated catalytic effectiveness factor. Unless specified otherwise, the simulations were conducted under the baseline scenario $\phi^2 = 4$, $\alpha_\infty = 0.65$, and $\lambda = 1.5$, indicative of a substantially diffusion-limited pellet experiencing gradual pore degradation.

The classical model is resolved utilising the Crank–Nicolson approach, while the variable-order fractional model is integrated by the fully implicit L1 scheme outlined in the preceding section. Both formulations are assessed under the same initial and boundary conditions, spatial discretization, and ultimate simulation duration, facilitating a direct comparison between the Fickian and non-Fickian models. The primary quantity of relevance is the transient effectiveness factor $\eta(\tau)$, as it offers a comprehensive assessment of internal reactant availability and immediately indicates the influence of intraparticle mass-transfer constraints on the observable reaction rate.

The numerical analysis is structured as follows. The concentration profiles forecasted by both models are analysed to demonstrate the impact of the changing fractional order on reactant infiltration into the pellet. The transient effectiveness factor is further examined to determine the time intervals during which the classical model overestimates catalyst performance. A parametric investigation is conducted about α_∞ and λ to ascertain the conditions under which the classical approximation remains valid and those in which the variable-order fractional formulation is essential for accurate reactor-scale predictions.

3.1 Spatial discretization

Both models are discretized on the uniform spatial grid

$$\xi_i = (i-1)\Delta\xi, \quad i = 1,\ldots,N_x, \quad \Delta\xi = \frac{1}{N_x - 1}. \tag{11}$$

The Laplacian operator $\partial^2 u/\partial\xi^2$ is approximated by the standard three-point central difference formula:

$$\left.\frac{\partial^2 u}{\partial \xi^2}\right|_{\xi_i} \approx \frac{u_{i-1}^k - 2u_i^k + u_{i+1}^k}{\Delta\xi^2} + \mathcal{O}(\Delta\xi^2). \tag{12}$$

The symmetry condition (4) at $i = 1$ (pellet center) is enforced via the ghost-node approach: $u_0^k = u_2^k$ for all k, which yields the modified stencil $(u_2^k - 2u_1^k + u_2^k)/\Delta\xi^2 = 2(u_2^k - u_1^k)/\Delta\xi^2$. The Dirichlet condition $u_{N_x}^k = 1$ is imposed explicitly at each time step.

3.2 Temporal discretization of M_{cl}: Crank-Nicolson scheme

The classical model (M_{cl}) is integrated in time with the Crank-Nicolson (CN) scheme, which is second-order accurate in time and unconditionally stable for parabolic equations:

$$\frac{u_i^{k+1} - u_i^k}{\Delta\tau} = \frac{1}{2}\left(\delta_\xi^2 u_i^{k+1} + \delta_\xi^2 u_i^k\right) - \frac{\phi^2}{2}\left(u_i^{k+1} + u_i^k\right), \tag{13}$$

where $\delta_\xi^2 u_i^k = (u_{i-1}^k - 2u_i^k + u_{i+1}^k)/\Delta\xi^2$. At each time step, (13) yields a symmetric tridiagonal linear system solved by the Thomas algorithm. The global truncation error is $\mathcal{O}(\Delta\tau^2 + \Delta\xi^2)$.

3.3 Temporal discretization of M_{vo}: Implicit L1 scheme

The Caputo VO derivative (7) is approximated by the L1 finite-difference formula (Sun *et al.*, 2019):

$${}^{C}D_{0,\tau}^{\alpha_{k+1}} u_i \approx \frac{\Delta\tau^{-\alpha_{k+1}}}{\Gamma(2-\alpha_{k+1})}\left[\left(u_i^{k+1} - u_i^k\right) + \sum_{j=1}^{k-1}\left(u_i^{k+1-j} - u_i^{k-j}\right)\omega_j^{(k)}\right]. \tag{14}$$

where $\alpha_{k+1} = \alpha(\tau_{k+1})$ and the non-negative memory weights are

$$\omega_j^{(k)} = (j+1)^{1-\alpha_{k+1}} - j^{1-\alpha_{k+1}}, \quad j = 1, 2, \ldots, k-1. \tag{15}$$

Note that $\omega_j^{(k)} > 0$ for all j and $\omega_j^{(k)} \searrow 0$ as $j \to \infty$, consistent with the power-law decay of memory in subdiffusive processes.

Derivation of the algebraic system. Let $\gamma_k = \Delta\tau^{\alpha_{k+1}}\,\Gamma(2-\alpha_{k+1})$ be the temporal scaling factor and define the history (memory) term

$$\mathcal{M}_i^k = \sum_{j=1}^{k-1} \left(u_i^{k+1-j} - u_i^{k-j}\right)\omega_j^{(k)}. \tag{16}$$

Substituting (14) into the spatial discretization of ($\mathrm{M_{vo}}$) and rearranging, the unknown u_i^{k+1} satisfies:

$$\left(1 + \frac{2\gamma_k}{\Delta\xi^2} + \gamma_k\phi^2\right)u_i^{k+1} - \frac{\gamma_k}{\Delta\xi^2}\left(u_{i-1}^{k+1} + u_{i+1}^{k+1}\right) = u_i^k - \mathcal{M}_i^k + s_i. \tag{17}$$

for $i = 1, \ldots, N_x - 1$, where $s_i = (\gamma_k/\Delta\xi^2)\cdot\mathbf{1}_{[i=N_x-1]}$ accounts for the contribution of the known boundary value $u_{N_x}^{k+1} = 1$. The coefficient matrix of (17) is tridiagonal, diagonally dominant, and independent of the solution; it is thus solved efficiently by the Thomas algorithm at each step.

Remark on consistency. As $\alpha_{k+1} \to 1$, we have $\Gamma(2-\alpha_{k+1}) \to 1$ and $\omega_j^{(k)} \to 0$ for all j; consequently $\gamma_k \to \Delta\tau$, $\mathcal{M}_i^k \to 0$, and (17) reduces to the backward Euler discretization of ($\mathrm{M_{cl}}$). This confirms that the L1 scheme is a consistent generalization of the implicit Euler method.

Temporal accuracy. For a constant order α, the L1 scheme achieves $\mathcal{O}(\Delta\tau^{2-\alpha})$ accuracy in time and $\mathcal{O}(\Delta\xi^2)$ in space (Lin and Xu, 2007; Oldham and Spanier, 2002). For the variable-order case, the local truncation error is $\mathcal{O}(\Delta\tau^{2-\alpha(\tau_{k+1})})$, which degrades toward first order as $\alpha \to 1$ (fresh catalyst) and improves as $\alpha \to 0$.

3.4 *Memory storage and computational cost*

The L1 scheme requires storing the complete solution history $\{u^k\}_{k=0}^K$ to evaluate the memory term (16) at each new step. This represents $\mathcal{O}(N_t \times N_x)$ memory, which is feasible for the problem sizes considered here. The computational cost per time step is $\mathcal{O}(k \times N_x)$ (evaluation of the memory sum) plus $\mathcal{O}(N_x)$ (Thomas solver), yielding a total cost of $\mathcal{O}(N_t^2 \times N_x)$ — the standard overhead of long-memory fractional schemes (Sun *et al.*, 2019).

3.5 *Discretization parameters*

All simulations use $N_x = 81$ spatial nodes ($\Delta\xi = 0.0125$) and $N_t = 8000$ time steps over $\tau \in [0, 4]$ ($\Delta\tau = 5\times10^{-4}$). Grid-independence with respect to the spatial resolution was verified by refining to $N_x = 161$; the maximum change in $\eta(\tau)$ was less than 0.2% for both models. A coarser temporal resolution ($N_t = 800$, $\Delta\tau = 5\times10^{-3}$) was also compared against the reported $N_t = 8000$ results and reproduces the same transient effectiveness factors and peak relative errors reported below to within about 0.1 percentage points, confirming that the results are not sensitive to the specific choice of N_t in this range. The effectiveness factor is evaluated by the composite trapezoidal rule on the spatial grid.

4 Results and discussion

This section aims to compare numerical curves and analyse the physical implications of substituting the classical Fickian description with a variable-order fractional transport model. Special emphasis is placed on the brief phase during which catalyst deactivation alters internal pore accessibility, resulting in a discernible delay in reactant penetration. This phase is particularly significant from an engineering standpoint, as reactor design, catalyst loading, and regeneration scheduling typically rely on effectiveness factors that presume constant transport qualities throughout time.

Unless otherwise stated, the base-case parameters are $\phi^2 = 4$, $\alpha_\infty = 0.65$, and $\lambda = 1.5$. These values place the system in an intermediate regime of diffusion limitation and moderate deactivation severity, representative of a zeolitic catalyst undergoing coking in a fixed-bed reactor (Froment *et al.*, 2011; A. Zhokh and Strizhak, 2018).

4.1 *Concentration Profiles*

Figure 1 illustrates the dimensionless concentration profiles within the catalyst pellet at specified dimensionless times for both the classical diffusion-reaction model and the proposed variable-order fractional model. In both scenarios, the surface concentration is maintained at $u(1,\tau) = 1$, whereas the symmetry constraint at the pellet centre necessitates a zero

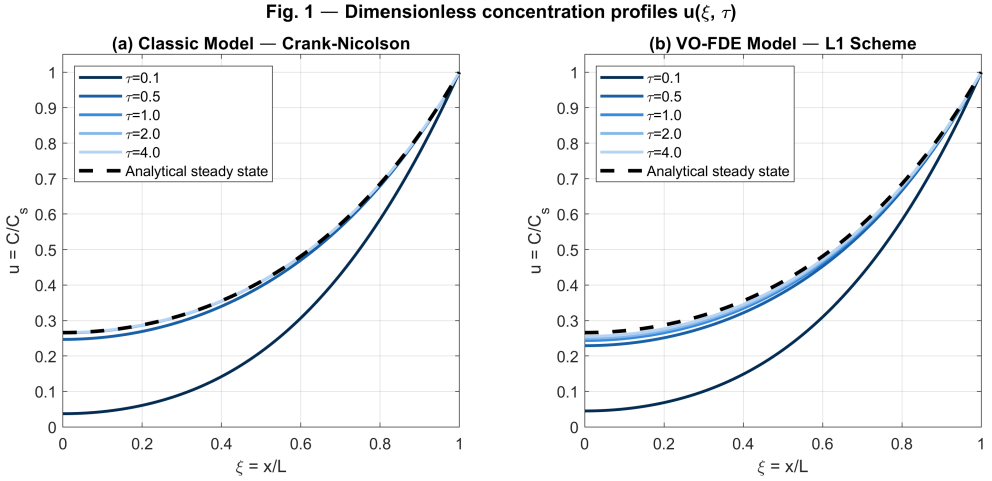

Fig. 1: Dimensionless reactant concentration profiles $u(\xi,\tau)$ at selected times $\tau = 0.1, 0.5, 1.0, 2.0, 4.0$ for (a) the classical model (M_{cl}) and (b) the VO-FDE model (M_{vo}), with $\phi^2 = 4$, $\alpha_\infty = 0.65$, and $\lambda = 1.5$. Dashed lines in both panels correspond to the analytical steady-state solution $u_\infty(\xi) = \cosh(\phi\xi)/\cosh\phi$.

concentration gradient at $\xi = 0$. As anticipated for a first-order reaction exhibiting internal diffusion constraints, the minimal concentration values are found around the pellet centre, where reactant ingress is most impeded. The dashed curve represents the analytical steady-state solution, $u_\infty(\xi) = \cosh(\phi\xi)/\cosh\phi$, which acts as the asymptotic reference profile for both formulations.

The classical Crank-Nicolson solution demonstrates a more rapid convergence to the steady-state profile. At an initial time, $\tau = 0.1$, the concentration within the pellet interior remains low, signifying that the reactant has only partially infiltrated the porous matrix. As time advances, the concentration field incrementally increases and converges towards the analytical steady state. Conversely, the VO-FDE model resolved using the implicit L1 scheme demonstrates a protracted transient response, especially at intermediate intervals. This behaviour results directly from the variable-order fractional derivative, which incorporates memory effects linked to anomalous subdiffusion. As $\alpha(\tau)$ diminishes from unity towards α_∞, the effective transport mechanism becomes less rapid than the standard Fickian forecast.

From an engineering perspective, the disparity between the two panels of Fig. 1 suggests that the classical model may overstate the internal availability of reactants during the temporary deactivation phase. While both models converge to the same steady-state concentration profile under the current assumptions, their transient routes differ. The VO-FDE formulation forecasts a postponed redistribution of reactants within the pellet, indicating a diminished volume-averaged concentration and, as a result, a decreased transient efficacy factor. Consequently, the concentration profiles in Fig. 1 offer the initial visual confirmation that progressive transport anomalies can substantially influence the anticipated efficacy of a deactivating porous catalyst.

Figure 1 depicts the temporal progression of the dimensionless concentration field within the catalyst pellet for both the classical and VO-FDE models. In both instances, the reactant concentration remains constant at the external surface and diminishes towards the centre of the pellet due to internal diffusion resistance and first-order consumption. At brief intervals, the concentration profiles deviate significantly from the analytical steady state, suggesting restricted reactant diffusion into the pellet's interior. As time progresses, the profiles increasingly converge towards the stationary solution.

A significant distinction between the two formulations is evident in the transitory route. The classical model attains the steady-state profile more swiftly, while the VO-FDE model forecasts a more gradual internal redistribution of reactants. The delay is linked to the memory effect caused by the variable-order fractional derivative, which signifies the shift from normal diffusion to anomalous subdiffusion when the catalyst becomes deactivated. Consequently, while both models converge to the identical stationary profile under the current assumptions, the VO-FDE model exhibits a more gradual and physically conservative transient behaviour.

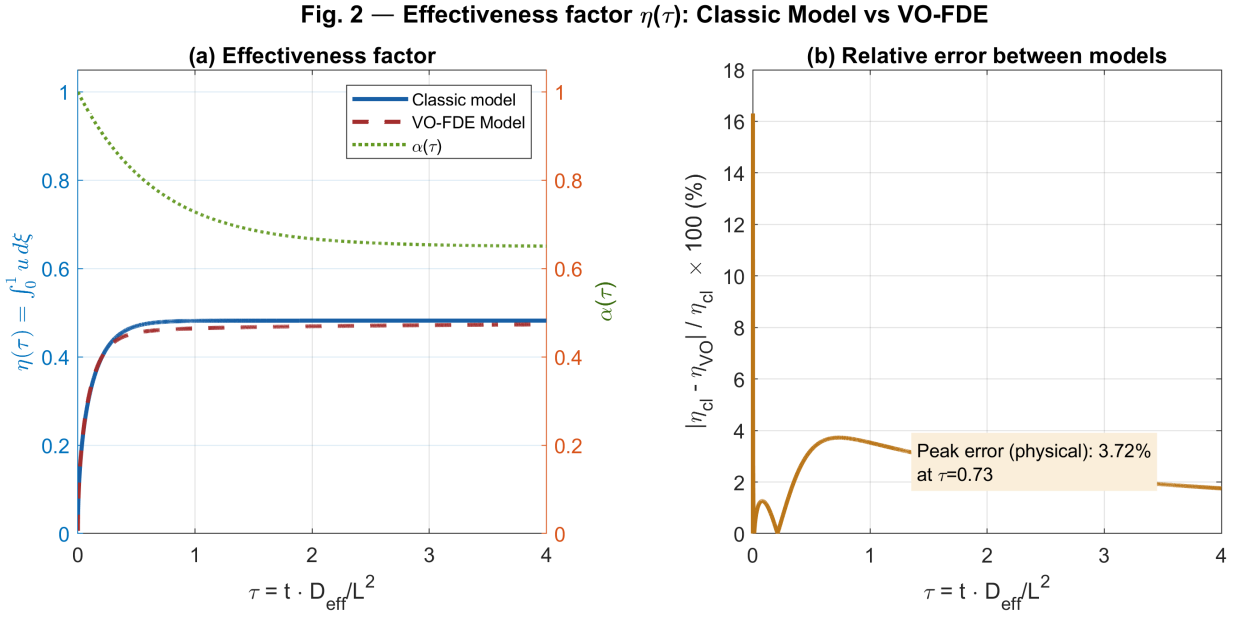

Fig. 2: (a) Transient effectiveness factor $\eta(\tau)$ for the classical model (M_{cl}, solid line) and the VO-FDE model (M_{vo}, dashed line), with the variable order $\alpha(\tau)$ shown on the right axis (dotted line). (b) Relative deviation $|\eta_{cl}-\eta_{vo}|/\eta_{cl}$ between both models as a function of τ. Parameters: $\phi^2 = 4$, $\alpha_\infty = 0.65$, and $\lambda = 1.5$.

Table 2. Effectiveness factor $\eta(\tau)$ predicted by the classical model (M_{cl}) and the VO-FDE model (M_{vo}) at selected dimensionless times. Parameters: $\phi^2 = 4$, $\alpha_\infty = 0.65$, and $\lambda = 1.5$.

τ	$\alpha(\tau)$	η_{cl}	η_{vo}	Error (%)
0.50	0.8153	0.46986	0.45457	3.26
1.00	0.7281	0.48157	0.46457	3.53
2.00	0.6674	0.48205	0.46936	2.63
4.00	0.6509	0.48205	0.47360	1.75

Error $= 100|\eta_{cl}-\eta_{vo}|/\eta_{cl}$. For $\phi^2 = 4$, $\eta_\infty = \tanh(2)/2 = 0.4820$.

4.2 *Transient effectiveness factor and model comparison*

Following the analysis of local concentration profiles, the comparison between the two formulations is broadened to include the transient catalyst efficacy component. This quantity offers a comprehensive assessment of reactant availability within the pellet and directly reflects the influence of internal diffusion constraints on the measured reaction rate. Consequently, $\eta(\tau)$ serves as an appropriate engineering metric to assess the validity of the classical Fickian model during catalyst ageing, or to determine the necessity of a variable-order fractional formulation. This subsection compares the effectiveness factors predicted by the classical and VO-FDE models over time, utilising the relative deviation between them to quantify the mistake resulting from disregarding anomalous subdiffusive transport.

Figure 2 compares the transient effectiveness factors predicted by both models. Table 2 reports the numerical values of η_{cl}, η_{vo}, and the relative deviation at selected times.

Three temporal regimes can be identified from Fig. 2 and Table 2:

Early regime ($\tau \lesssim 0.1$). At very short times, $\alpha(\tau) \approx 1$ and the VO-FDE model reduces to the classical model; both curves coincide. This confirms the self-consistency of the proposed framework (Eq. (8), $\alpha(0) = 1$). It is worth noting that the *relative* deviation $|\eta_{cl} - \eta_{vo}|/\eta_{cl}$ plotted in Fig. 2b is numerically ill-conditioned in this regime: both η_{cl} and η_{vo} start from zero (Eq. (3)), so the denominator η_{cl} is itself vanishingly small as $\tau \to 0$. Any residual, physically negligible absolute difference between the two curves is therefore amplified into a large percentage error near $\tau = 0$, even though the two solutions are, by construction, essentially identical there. This early-time spike is a normalization artifact of the relative-error metric rather than evidence of a genuine model discrepancy, and it is excluded from the discussion of the physically meaningful error below.

Intermediate regime ($0.1 \lesssim \tau \lesssim 2.0$). As $\alpha(\tau)$ decreases from unity, the VO-FDE model

predicts a slower approach to steady state compared to the classical model. Once the early-time artifact discussed above has decayed, the physically meaningful relative deviation reaches its maximum of 3.74% at $\tau \approx 0.73$, where $\alpha(\tau) \approx 0.75$ — a point lying between the two tabulated instants $\tau = 0.5$ (3.26%) and $\tau = 1.0$ (3.53%) in Table 2, consistent with the monotonic rise and fall of the error bracketing it. This location of the peak is physically consistent: at very short times both models still coincide ($\alpha \approx 1$), while at long times both converge to the same steady state; the maximum disagreement must therefore occur at an intermediate time, once the memory kernel of the VO-FDE model has accumulated enough weight to measurably retard reactant penetration, but before the concentration field has had time to relax back toward the common steady profile. Subdiffusion ($\alpha < 1$) implies a slower transport of reactant into the pellet interior, leading to a lower time-averaged concentration and thus a lower effectiveness factor.

Long-time regime ($\tau \gtrsim 2.0$). Both models converge toward the same steady state $\eta_\infty = \tanh\phi/\phi$, since, in the limit $\tau \to \infty$, both formulations approach the same time-independent (steady) concentration profile: the governing PDE remains formally parabolic for any finite τ irrespective of the fractional order, but its solution becomes stationary as $\tau \to \infty$, at which point it satisfies the same elliptic boundary-value problem obtained by setting the time derivative to zero in either model. Consistent with this, the relative error decreases monotonically from its peak of 3.74% near $\tau \approx 0.73$ down to 1.75% at $\tau = 4.0$ (Table 2).

4.3 *Parametric study: effect of α_∞ and λ*

A parametric research was conducted to assess the impact of the two principal deactivation-related parameters of the VO-FDE model: the asymptotic fractional order α_∞ and the transition rate λ, following the comparison of the base-case response. The parameter α_∞ dictates the ultimate degree of anomalous subdiffusion attained by the aged catalyst, while λ governs the rate at which the system transitions from the initial Fickian phase to the subdiffusive regime. Consequently, these factors enable the model to depict various deactivation scenarios, from mild and slow pore degradation to severe and rapid transport deterioration.

The analysis examines how alterations in α_∞ and λ influence the transient effectiveness factor $\eta(\tau)$ and the divergence from the standard diffusion-reaction model. This comparison is helpful in determining the operational settings where the classical Fickian approximation is sufficient and where the variable-order fractional formulation is essential for accurately depicting catalyst performance with progressive ageing.

Figure 3 illustrates the impact of the asymptotic fractional order α_∞ on the transient effectiveness factor. This parameter regulates the ultimate extent of anomalous transport attained by the deactivate catalyst. Values of α_∞ approaching unity indicate somewhat impacted porous materials, wherein the transport mechanism remains roughly Fickian. Conversely, diminished values of α_∞ signify enhanced subdiffusive behaviour, linked to pore obstruction, heightened tortuosity, or diminished connectivity within the internal pore network.

As illustrated in Fig. 3a, all VO-FDE curves converge to a similar efficacy range; nevertheless, their temporary progression is contingent upon the chosen value of α_∞. The scenario $\alpha_\infty = 0.95$ closely aligns with classical predictions, affirming that the integer-order model is suitable when the catalyst undergoes minimal transport degradation. As α_∞ diminishes to 0.80, 0.65, and 0.50, the efficacy factor correspondingly declines throughout the transitory phase. This suggests that enhanced anomalous diffusion postpones the internal redistribution of the reactant and diminishes the volume-averaged concentration within the pellet.

Because at $\tau_{\text{end}} = 4$ both models are already close to the common steady state $\eta_\infty = \tanh\phi/\phi$, the absolute spread of the curves in Fig. 3a at the final time is small. Expressed instead as a percentage change relative to the classical value, Fig. 3b shows that the final-time effectiveness factor departs from the classical prediction by −0.16%, −0.81%, −1.75%, and −2.99% for $\alpha_\infty = 0.95, 0.80, 0.65, 0.50$, respectively (i.e., under about 3% even for the most severe case considered), confirming quantitatively that the ultimate (steady-state) effectiveness factor is only weakly sensitive to α_∞ over the simulated time window compared with the much larger transient (peak) deviations documented below. This is consistent with the fact that, under the present assumptions, the stationary diffusion-reaction problem is governed by the same spatial operator regardless of α_∞. Consequently, the primary contribution of the variable-order

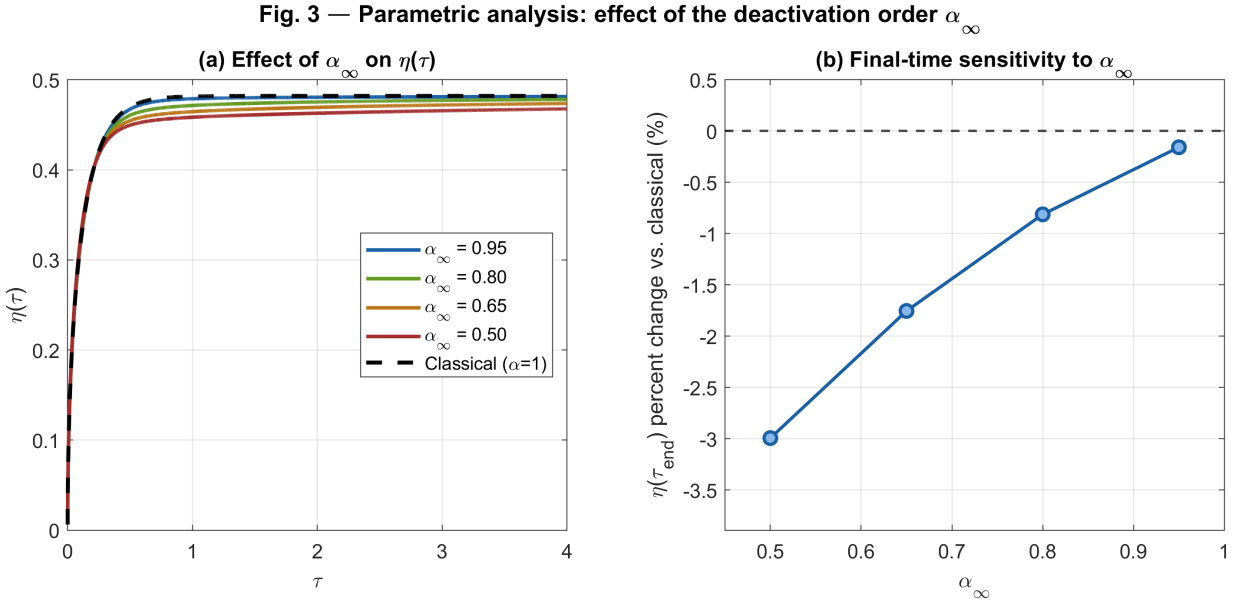

Fig. 3: (a) Transient effectiveness factor $\eta(\tau)$ for four values of $\alpha_\infty \in \{0.50, 0.65, 0.80, 0.95\}$ using the VO-FDE model, compared with the classical model. (b) Percentage change of the final-time effectiveness factor relative to the classical value, $100\,[\eta(\tau_{end}) - \eta_{cl}(\tau_{end})]/\eta_{cl}(\tau_{end})$, as a function of α_∞, shown with an expanded ordinate scale to resolve the magnitude of this comparatively small effect. Parameters: $\phi^2 = 4$ and $\lambda = 1.5$.

Table 3. Peak relative deviation between the classical and VO-FDE effectiveness factors as a function of α_∞ (base case $\phi^2 = 4$, $\lambda = 1.5$).

α_∞	Peak error (%)
0.95	0.67
0.90	1.24
0.80	2.31
0.65	3.74
0.50	4.97

model is not to alter the traditional steady-state effectiveness factor, but to elucidate the slower transient pathway undertaken by a progressively deactivating catalyst. From a design standpoint, this ephemeral discrepancy is significant, as reactor performance may be overestimated if the classical model is applied while the catalyst is undergoing active ageing.

Threshold for classical model validity. Table 3 reports the peak relative deviation between the VO-FDE and classical models over the full transient (excluding the early-time normalization artifact discussed above), for $\lambda = 1.5$ and $\alpha_\infty \in \{0.95, 0.90, 0.80, 0.65, 0.50\}$. For $\alpha_\infty \geq 0.90$ (mild deactivation), the peak relative deviation remains below 1.5% (0.67% and 1.24% for $\alpha_\infty = 0.95$ and 0.90, respectively),

Table 4. Effect of the deactivation rate λ on the peak relative deviation between the classical and VO-FDE effectiveness factors. Parameters: $\phi^2 = 4$, $\alpha_\infty = 0.65$.

λ	τ^* (peak location)	Peak error (%)
0.5	0.82	1.85
1.0	0.78	2.99
1.5	0.73	3.74
3.0	0.66	4.84

and the classical model constitutes an acceptable engineering approximation. For $\alpha_\infty \leq 0.80$ (moderate to severe deactivation), the peak deviation exceeds 2% and grows to nearly 5% at $\alpha_\infty = 0.50$, so the VO-FDE model is recommended for accurate prediction of $\eta(\tau)$.

Effect of deactivation rate λ. To quantify the role of λ, the same base case ($\phi^2 = 4$, $\alpha_\infty = 0.65$) was re-solved for $\lambda \in \{0.5, 1.0, 1.5, 3.0\}$, and the peak relative deviation $\max_\tau |\eta_{cl} - \eta_{vo}|/\eta_{cl}$ together with the time τ^* at which it occurs were extracted for each case (Table 4). As λ increases from 0.5 to 3.0, $\alpha(\tau)$ approaches α_∞ more rapidly (Eq. (8)), so the memory kernel accumulates subdiffusive weight earlier in the simulation: the peak deviation is reached at a progressively smaller τ^* (from 0.82 down to 0.66) while its magnitude increases from 1.85% to 4.84%, confirming quantitatively, and not

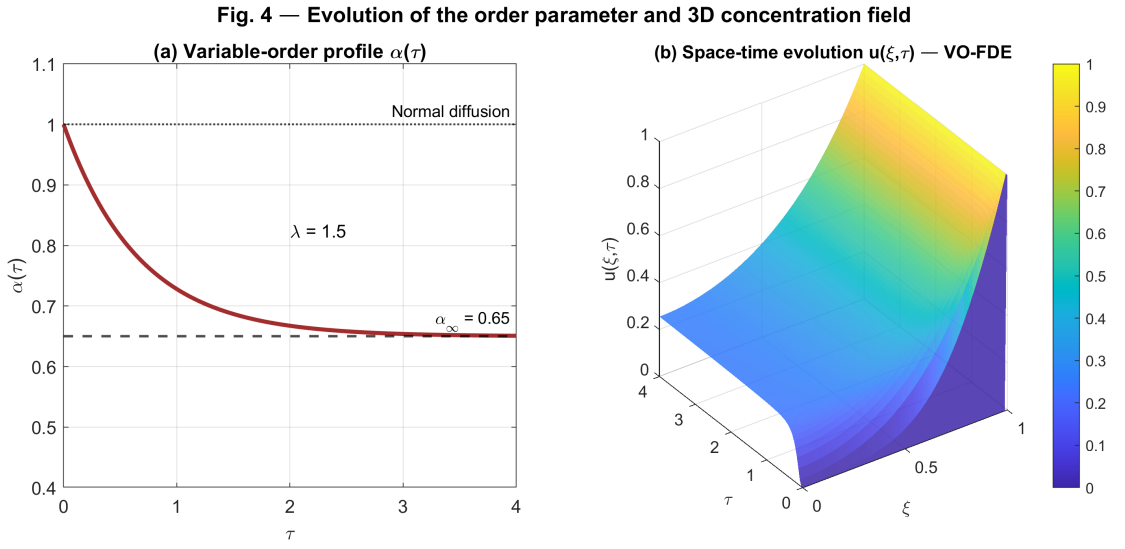

Fig. 4: (a) Time evolution of the variable order $\alpha(\tau)$ for the base case, with $\alpha_\infty = 0.65$ and $\lambda = 1.5$. (b) Three-dimensional surface plot of the dimensionless concentration field $u(\xi, \tau)$ predicted by the VO-FDE model (M_{vo}).

only qualitatively, that a larger λ both advances and intensifies the transient deviation from the classical model. A small λ corresponds to gradual fouling: the transition of $\alpha(\tau)$ toward α_∞ is slow, so the peak deviation is smaller in magnitude and occurs later, consistent with the early- and intermediate-regime description of Section *4.2*.

4.4 Space-time visualization and the role of the memory kernel

This subsection analyses the comprehensive space-time behaviour of the VO-FDE solution, supplementing the prior one-dimensional profiles and integral effectiveness-factor analysis. The aim is to illustrate how the time-dependent fractional order alters the propagation of reactant concentration within the pellet and to emphasise the function of the memory kernel in postponing the transitory response.

The three-dimensional surface in Fig. 4b reveals the non-trivial space-time coupling introduced by the variable-order operator. At early times ($\alpha \approx 1$), isoconcentration lines are closely spaced near the surface and spread slowly toward the center, consistent with normal diffusion. At intermediate times, as α decreases, the propagation of concentration into the pellet interior slows down noticeably relative to the classical parabolic envelope. At late times, the surface approaches the steady-state profile $\cosh(\phi\xi)/\cosh\phi$ from below, with the VO-FDE solution converging more slowly than the classical counterpart.

Role of the memory kernel. A distinctive feature of the L1 scheme is the accumulation of history weights $\omega_j^{(k)}$ [Eq. (15)]. At each time step $k+1$, the memory term $\mathcal{M}_i^k$ [Eq. (16)] incorporates contributions from all previous increments $u^{k+1-j} - u^{k-j}$, weighted by a decreasing power-law. This non-local coupling is the mathematical signature of the trapping phenomena responsible for subdiffusion in porous media, and its neglect (as in the classical model) leads to the systematic overestimation of $\eta(\tau)$ documented in Section *4.2*.

5 Conclusions

This work proposed, implemented, and analyzed a variable-order fractional differential equation (VO-FDE) model for isothermal diffusion-reaction in a flat-slab porous catalyst pellet undergoing progressive deactivation, with $\alpha(\tau)$ governed by the exponential law $\alpha(\tau) = \alpha_\infty + (1 - \alpha_\infty)e^{-\lambda\tau}$ and solved with an implicit L1 scheme benchmarked against the classical Crank–Nicolson solution. Beyond confirming that the VO-FDE model is a consistent generalization of the classical one (both coincide as $\tau \to 0$ and as $\alpha_\infty \to 1$, and both approach the same Thiele steady state $\eta_\infty = \tanh\phi/\phi$), the numerical experiments yield three findings that were not evident *a priori*. First, the classical model does not overestimate the effectiveness factor uniformly in time: the relative deviation between models is

negligible at very short and very long times and instead peaks at an intermediate time ($\tau^* \approx 0.73$ for the base case, where the error reaches 3.74%), because the memory kernel of the VO-FDE model needs a finite time to accumulate enough weight to measurably retard reactant penetration before both solutions relax toward the shared steady state; the strong percentage spike sometimes visible at $\tau \to 0$ in the relative-error curve is a normalization artifact of dividing by a vanishingly small η_{cl}, not a genuine discrepancy, and should not be mistaken for the physically meaningful peak. Second, α_∞ and λ affect the transient response in distinct and separable ways: α_∞ mainly controls the *magnitude* of the deviation window (peak error below 1.5% for $\alpha_\infty \geq 0.90$, rising above 2% and reaching nearly 5% as α_∞ decreases to 0.80 and 0.50, respectively), while λ mainly controls *when* the peak deviation occurs and how quickly it develops, with faster deactivation (larger λ) producing an earlier and sharper peak rather than simply a larger one. Third, because the steady-state effectiveness factor is governed by the same spatial (elliptic) operator regardless of α_∞, the ultimate, long-time performance of the catalyst is only weakly sensitive to the degree of anomalous transport; the practical consequence of the VO-FDE formulation is therefore concentrated in the intermediate-life transient window relevant to reactor sizing and regeneration scheduling, rather than in the asymptotic design value η_∞ conventionally used in classical reactor calculations.

From a practical engineering perspective, the additional complexity of the VO-FDE formulation is not necessarily justified whenever the difference from the classical model is small. Within the parameter range investigated here, the maximum physically meaningful deviation remains below approximately 5%. Therefore, for preliminary design, steady-state calculations, or applications in which experimental and parameter uncertainties are of comparable or greater magnitude, the classical model remains the more parsimonious and computationally efficient choice. The variable-order formulation becomes more relevant when transient deviations of only a few percent can alter an operational decision, for example in catalyst-lifetime prediction, regeneration scheduling based on performance thresholds, dynamic optimization under changing operating conditions, or high-accuracy digital twins used for state estimation and predictive operation. In such applications, a systematic transient bias of 2–5% may shift the predicted time at which a catalyst reaches a performance or regeneration threshold. Conversely, when the uncertainty of the available measurements or identified parameters exceeds the discrepancy between the two models, the additional computational and parameter-identification burden of the VO-FDE formulation would not be warranted.

A practical caveat that follows directly from these results concerns model identifiability. The VO-FDE formulation introduces two additional parameters, α_∞ and λ, relative to the single Thiele modulus ϕ^2 required by the classical model, and Section *4.3* shows that these two parameters affect the transient response in different, only partially separable ways (magnitude versus timing of the peak deviation). Estimating α_∞, λ, and D_{eff} simultaneously by regression against a single transient concentration or uptake curve is therefore an ill-conditioned inverse problem in general, and parameter estimates obtained this way should be interpreted with caution unless the data set independently constrains at least one of the three quantities (for example, D_{eff} from a fresh-catalyst experiment before deactivation begins, or α_∞ from a long-time asymptotic measurement on a fully aged catalyst). Regression against pellet-averaged data of the type used here is also blind to any spatial heterogeneity in pore accessibility, so an experimental program aimed at identifying these parameters should combine transient effectiveness-factor or uptake measurements with at least one spatially or texturally resolved diagnostic (e.g., intraparticle concentration mapping or pore-size-distribution evolution) if the underlying multiscale trapping process is to be captured reliably; this additional experimental burden, relative to the single Thiele modulus needed by the classical model, is the main practical cost of adopting the variable-order description.

Future work. Extensions of the present framework include: (i) generalization to spherical pellet geometry and non-isothermal conditions; (ii) incorporation of concentration-dependent kinetics (e.g., Langmuir-Hinshelwood); (iii) coupling of the variable order to a mechanistic coking kinetics model Bartholomew, 2001; (iv) experimental validation using transient concentration profiles measured by *in situ* MRI or neutron scattering techniques; (v) embedding of the VO-FDE pellet model within a one-dimensional fixed-bed reactor model to study the axial propagation of deactivation fronts; and (vi) extension of the fractional order to a space-time field $\alpha(\xi, \tau)$ that would also capture the spatial

heterogeneity of pore blockage discussed in Section 1, together with an identifiability analysis to establish which combinations of transient and spatially resolved data are required to constrain such a model.

Acknowledgements

The authors acknowledge the support of the Tecnológico Nacional de México through the 2026 Research Projects Call under the project "Plataforma automatizada de control, inteligencia artificial y observadores de estado avanzados para la valorización de componentes bioasimilables mediante oxidación avanzada y fotobiorreactores." Additionally, the first author gratefully acknowledges the support provided by Universidad Tecnológica de México (UNITEC).

References

Aris, R. (1975). *The mathematical theory of diffusion and reaction in permeable catalysts* (Vol. 1 and 2). Clarendon Press.

Bartholomew, C. H. (2001). Mechanisms of catalyst deactivation. *Applied Catalysis A: General*, *212*, 17–60. https://doi.org/10.1016/S0926-860X(00)00843-7

Birbal, C. V., Martinez, S., & Castro, Y. (2025). Enhancing heavy crude oil recovery: Injection of FeNi nanoparticles with steam into porous medium. *Revista Mexicana de Ingeniería Química*, *24*(1), Proc24389. https://doi.org/10.24275/rmiq/Proc24389

Bouchaud, J. P., & Georges, A. (1990). Anomalous diffusion in disordered media: Statistical mechanisms, models and physical applications. *Physics Reports*, *195*, 127–293. https://doi.org/10.1016/0370-1573(90)90099-N

Chechkin, A. V., Gorenflo, R., & Sokolov, I. M. (2005). Fractional diffusion in inhomogeneous media. *Journal of Physics A: Mathematical and General*, *38*, L679–L684. https://doi.org/10.1088/0305-4470/38/42/L03

Cho, Y. (2022). Analytical solutions of reaction–diffusion phenomena by porous cylindrical pellets with finite length. *The Canadian Journal of Chemical Engineering*, *101*(6), 3431–3461. https://doi.org/10.1002/cjce.24700

Cho, Y.-S. (2023). Modeling of Porous Catalytic Pellets with Various Morphologies Suspended in Batch Reactor and CSTR from Analytical Solutions of Reaction-Diffusion Equations. *Journal of Chemical Engineering of Japan*, *56*(1). https://doi.org/10.1080/00219592.2023.2247783

Coimbra, C. F. M. (2003). Mechanics with variable-order differential operators. *Annalen der Physik*, *12*, 692–703. https://doi.org/10.1002/andp.200310032

Cortés-Avendaño, E. J., Castillo-Zamudio, R. I., Salgado-Cervantes, M. A., & García-Alvarado, M. A. (2023). Heat and mass transfer heterogeneous model applied for mathematical representation of Aloe vera extracts spray drying. *Revista Mexicana de Ingeniería Química*, *22*(2), Alim237. https://doi.org/10.24275/rmiq/Alim237

Dabiri, A., Moghaddam, B. P., & Machado, J. A. T. (2018). Optimal variable-order fractional pid controllers for dynamical systems. *Journal of Computational and Applied Mathematics*, *339*, 40–48. https://doi.org/10.1016/j.cam.2018.02.029

Fogler, H. S. (2016). *Elements of chemical reaction engineering* (5th ed.). Prentice Hall.

Froment, G. F., Bischoff, K. B., & De Wilde, J. (2011). *Chemical reactor analysis and design* (3rd ed.). Wiley.

Hernández Aguirre, A., Morales-Cabrera, M., Morales-Zárate, E., Rivera, V., Puebla, H., & Hernández-Martínez, E. (2017). Non-isothermal effectiveness factor for catalytic particles with non-fickian diffusion. *International Journal of Chemical Reactor Engineering*, *15*(5), 20170024. https://doi.org/10.1515/ijcre-2017-0024

Hernández-Martínez, E., Puebla, H., Valdés-Parada, F. J., & Álvarez-Ramírez, J. (2016). A green's function approach for the numerical solution of a class of fractional reaction-diffusion equations. *Mathematics and Computers in Simulation*, *121*, 133–145. https://doi.org/10.1016/j.matcom.2015.09.004

Hong, J., Jin, B., & Kian, Y. (2024). Identification of a Spatially-Dependent Variable Order in One-Dimensional Subdiffusion.

Keil, F. J. (2012). Diffusion and reaction in porous networks. *Catalysis Today*, *53*, 245–258. https://doi.org/10.1016/S0920-5861(99)00119-4

Kilbas, A. A., Srivastava, H. M., & Trujillo, J. J. (2006). *Theory and applications of fractional differential equations*. Elsevier.

Levenspiel, O. (1998). *Chemical reaction engineering* (3rd ed.). Wiley.

Lin, Y., & Xu, C. (2007). Finite difference/spectral approximations for the time-fractional diffusion equation. *Journal of Computational Physics*, *225*, 1533–1552. https://doi.org/10.1016/j.jcp.2007.02.001

Lorenzo, C. F., & Hartley, T. T. (2002). Variable order and distributed order fractional operators. *Nonlinear Dynamics*, *29*, 57–98. https://doi.org/10.1023/A:1016586905654

Martínez-Hilario, D. G., Carrasco-Venegas, L. A., González-Fernández, J. V., Soto-Gonzales, J. L., & Carranza-Oropeza, M. V. (2023). Modeling NPK nutrients release via nanoparticle/hydrogel system. *Revista Mexicana de Ingeniería Química*, *22*(2), Sim2399. https://doi.org/10.24275/rmiq/Sim2399

Martínez-Martínez, F., Rivera, V. M., Morales-Cabrera, M. A., & Hernández-Martínez, E. (2016). Dynamic effectiveness factor for catalytic particles with anomalous diffusion. *International Journal of Chemical Reactor Engineering*, *14*(6), 1235–1240. https://doi.org/10.1515/ijcre-2015-0221

Melgarejo-Torres, R., Rosales-Mercado, D., Polo-Labarrios, M. A., Fernández-Anaya, G., Morales-Ibarría, M., Pérez-Vega, S. B., Arce-Vázquez, M. B., & Palmerín-Carreño, D. M. (2022). Mathematical model to estimate volumetric oxygen transfer coefficient in bioreactors using conformable calculus. *Revista Mexicana de Ingeniería Química*, *21*(2), Bio2701. https://doi.org/10.24275/rmiq/Bio2701

Metzler, R., & Klafter, J. (2000). The random walk's guide to anomalous diffusion: A fractional dynamics approach. *Physics Reports*, *339*, 1–77. https://doi.org/10.1016/S0370-1573(00)00070-3

Moghaddama, M., Abbassi, A., & Ghazanfarian, J. (2022). Microstructure Effects on Performance and Deactivation of Hierarchically Structured Porous Catalyst: A Pore Network Model. *Social Science Research Network*. https://arxiv.org/pdf/2202.02720. https://doi.org/10.2139/ssrn.4030241

Moulijn, J. A., van Diepen, A. E., & Kapteijn, F. (2001). Catalyst deactivation: Is it predictable? what to do? *Applied Catalysis A: General*, *212*, 3–16. https://doi.org/10.1016/S0926-860X(00)00842-5

Obembe, A. D., Hossain, M. E., & Abu-Khamsin, S. A. (2017). Variable-order derivative time fractional diffusion model for heterogeneous porous media. *Journal of Petroleum Science and Engineering*, *152*, 391–405. https://doi.org/10.1016/j.petrol.2017.03.015

Oldham, K. B., & Spanier, J. (2002). *The fractional calculus: Theory and applications of differentiation and integration to arbitrary order*. Dover.

Podlubny, I. (1999). *Fractional differential equations*. Academic Press.

Rajaraman, R. (2024). Exploring nonlinear reaction–diffusion in enzyme immobilized systems: Integer and fractional order modeling. *Applied Biochemistry and Biotechnology*, *197*(2), 793–820. https://doi.org/10.1007/s12010-024-05050-x

Samko, S. G., & Ross, B. (1993). Integration and differentiation to a variable fractional order. *Integral Transforms and Special Functions*, *1*, 277–300. https://doi.org/10.1080/10652469308819027

Sobhani, H., Azimi, A., Noghrehabadi, A., & Mozafarifard, M. (2023). Numerical study and parameters estimation of anomalous diffusion process in porous media based on variable-order time fractional dual-phase-lag model. *Numerical Heat Transfer, Part A: Applications*, *83*(7), 679–710. https://doi.org/10.1080/10407782.2022.2157915

Sun, H., Chang, A., Zhang, Y., & Chen, W. (2019). A review on variable-order fractional differential equations: Mathematical foundations, physical models, numerical methods and applications. *Fractional Calculus and Applied Analysis*, *22*, 27–59. https://doi.org/10.1515/fca-2019-0003

Thiele, E. W. (1939). Relation between catalytic activity and size of particle. *Industrial & Engineering Chemistry*, *31*, 916–920. https://doi.org/10.1021/ie50355a027

Valdés-Parada, F. J., Wood, B. D., & Whitaker, S. (2023). Fick's law: A derivation based on continuum mechanics. *Revista Mexicana de Ingeniería Química*, *22*(3), Fen23102. https://doi.org/10.24275/rmiq/Fen23102

Wen, J., Ren, G., Yu, Y., Wang, K., He, J., Chen, Y., Yan, X., Guo, Q., & Li, J. (2024). A non-linear diffusion of amorphous Pt

studied using a variable-order fractional model. *Physica B: Condensed Matter*, *673*, 415448. https://doi.org/10.1016/j.physb.2023.415448

Zeldovich, Y. B. (1939). On the theory of reactions on powders and porous substances. *Acta Physicochim. URSS*, *10*, 583.

Zhang, M., & Liu, F. (2023). Fractional diffusion model generalised by the distributed-order operator involving variable diffusion coefficients. *ANZIAM Journal*, *64*. https://doi.org/10.21914/anziamj.v64.17959

Zhokh, A., & Strizhak, P. (2018). Non-fickian transport in porous media: Always temporally anomalous? *Transport in Porous Media*, *124*, 309–323. https://doi.org/10.1007/s11242-018-1066-6

Zhokh, A., & Strizhak, P. (2019). Investigation of the anomalous diffusion in the porous media: A spatiotemporal scaling. *Heat and Mass Transfer*, *55*, 2693–2702. https://doi.org/10.1007/s00231-019-02602-4

Zhokh, O. (2024). Modeling catalyst effectiveness factor with space-fractional derivative using Haar wavelet collocation method. *International Journal of Chemical Reactor Engineering*, *22*(9), 1101–1106. https://doi.org/10.1515/ijcre-2024-0128